

ELiSe: Efficient Learning of Sequences in Structured Recurrent Networks

Laura Kriener^{*,†,1,2}, Kristin Völk^{*,1,3},
Ben von Hünenbein¹, Federico Benitez¹, Walter Senn¹, Mihai A. Petrovici^{†,1}

* Shared first authorship

† Corresponding authors {laura.kriener,mihai.petrovici}@unibe.ch)

¹Department of Physiology, University of Bern, 3012 Bern, Switzerland.

²Institute of Neuroinformatics, University of Zurich and ETH Zurich, 8057 Zurich, Switzerland.

³Catlab Engineering GmbH, 82284 Grafrath, Germany.

September 30, 2024

Abstract

Behavior can be described as a temporal sequence of actions driven by neural activity. To learn complex sequential patterns in neural networks, memories of past activities need to persist on significantly longer timescales than the relaxation times of single-neuron activity. While recurrent networks can produce such long transients, training these networks is a challenge. Learning via error propagation confers models such as FORCE, RTRL or BPTT a significant functional advantage, but at the expense of biological plausibility. While reservoir computing circumvents this issue by learning only the readout weights, it does not scale well with problem complexity. We propose that two prominent structural features of cortical networks can alleviate these issues: the presence of a certain network scaffold at the onset of learning and the existence of dendritic compartments for enhancing neuronal information storage and computation. Our resulting model for Efficient Learning of Sequences (ELiSe) builds on these features to acquire and replay complex non-Markovian spatio-temporal patterns using only local, always-on and phase-free synaptic plasticity. We showcase the capabilities of ELiSe in a mock-up of birdsong learning, and demonstrate its flexibility with respect to parametrization, as well as its robustness to external disturbances.

1 Introduction

Despite seeming mundane, everyday activities such as catching a ball, walking down a flight of stairs or whistling a tune are comprised of complex and precisely timed sequences of actions. These action sequences are grounded in corresponding spatio-temporal patterns of neural activity in motor and pre-motor areas. One prominent example of sequence learning and replay is song production in male zebra finches, who learn to reproduce the stereotypical vocalizations of their elders. After learning, the neural activity in the robust nucleus of the archistriatum (RA) pre-motor area is marked by sparse bursting that is closely linked to features in the song [1, 2]. A similarly action-coupled temporally precise activity has been observed following motor learning in mouse primary motor cortex [3, 4] and navigation learning in rat posterior parietal cortex [5].

A detailed model of these mechanisms at the computational level remains an open question. A key challenge for models of

sequence learning is to bridge the temporal gap between neural activity evolving at the timescale of milliseconds and the behaviour performed at the timescale of seconds. Typically, sustained dynamics in recurrently connected neuron populations are assumed to produce the required transients. The most straightforward way to exploit such activity is to learn a direct mapping to a readout population, as proposed by reservoir computing [6]. However, such reservoirs are rather sensitive to initial conditions, and incorrect initialization can lead to exploding or fading activity. Furthermore, this approach scales poorly to more complex tasks, as the readout must rely on useful transients being available within the otherwise random activity of the reservoir. It thus seems essential for stability and resource efficiency to solve the challenging problem of learning the recurrent weights themselves.

Multiple approaches for recurrent weight learning have been previously explored. Techniques from Machine Learning are not straightforward to apply, as they are often at odds with observed neurophysiology. Such constraints exclude otherwise powerful methods such as backpropagation through time (BPTT) [7] and real-time recurrent learning (RTRL) [8]. Approximations of RTRL such as random feedback online learning (RFLO) [9] improve its biological plausibility by reducing its memory requirements at the cost of approximating the propagated gradients. However, some locality issues remain: synaptic eligibility traces need to share time constants with afferent neurons, and correct transport of errors requires copying synaptic weights [9]. Other approaches further narrow the biological plausibility gap at the expense of requiring narrowly specified forms of error transport. Still, several important issues remain to be addressed. FORCE learning [10, 11] requires strong feedback connections and near-instantaneous plasticity capable of closely tracking any changes in neuronal activity. FOLLOW [12] partly alleviates this problem, but still relies on global error feedback to each neuron in the network.

A different approach [13] suggests the prior learning of a “clock” - a chain of recurrent modules that are activated in sequence. In a second phase, arbitrary sequences can then be learned as a simple one-to-one mapping from individual links in this chain to specific motor outputs at every point in time. While biologically plausible, this model requires large amounts of resources, as the clock chain must scale with the pattern length and complexity. Nonetheless, the effectiveness of this model indicates that emulating innate structures can

be advantageous for sequence learning, as opposed to learning that starts from a blank slate.

Indeed, there is overwhelming evidence for such a balance happening in biological brains, between the flexibility offered by experience-dependent plasticity and the effectiveness of hardwired structural adaptations to specific use cases [14]. The building of such scaffolding structures has been observed during development of several subsystems of the mammalian brain, such as cerebellum, hippocampus and cortex [15–17], as we discuss in more detail below.

Introducing biologically inspired components can often feel like constraining a computational model’s generality instead of aiding its functionality. In contrast, in our model of Efficient Learning of Sequences (ELiSe) we show that inductively biasing our model in two specific ways not only increases its biological plausibility but also serves to enhance its functionality. First, whereas deep learning builds on the training of randomly initialized neural networks – what can properly be called a *tabula rasa* – learning in the brain builds on pre-existing structures, shaped by eons of evolution and cast into genes. Here we suggest how such structures could form during early development, before any learning takes place, and how they can provide a better basis for recurrent learning and significantly eases the task of learning temporal sequences. Second, neurons in deep learning models, unlike cortical neurons, do not have an internal structure and serve as simple nonlinear transfer functions. However, it has been shown that the structured nature of biological neurons allows for much more complex information storage and computation within single neurons [18–22]. Inspired by these experimental results, we use a two-compartment extension to simple point neuron models, in conjunction with a local error-correcting plasticity rule. This alleviates the necessity for non-local quantities or global error signals in the learning mechanism. Taken together, the introduction of structure both in the network and in the model neurons themselves creates a versatile substrate for continuous, on-line sequence learning in the brain. Importantly, our model makes efficient use of its neuronal resources, allowing the learning of complex sequences with only a small number of neurons. We demonstrate these features in a mock-up of birdsong learning, in which our networks learn a long, non-Markovian¹ sequence (a sample of Beethoven’s “Für Elise”) that they can reproduce robustly despite severe external disturbances.

2 Model description

In evolved biological systems there is a close connection between function and form. When considering complex behavior, even if learning would start from some kind of *tabula rasa*, realistically it needs the right kind of *tabula* to be effective. In order to model this, it is essential to consider early brain development. For example, recent research [16] has shown that the functional organization of the adult hippocampus is not only formed through experience-dependent plasticity but partly hardwired at the earliest stages of development, includ-

¹We use “non-Markovian” as shorthand for “not 1st-order Markovian”.

ing embryonic neurogenesis. These developmental programs provide a scaffold onto which later experience of the external world can be grafted. This is reflected in the dynamics of the adult CA1 region of hippocampus, which operates through a combination of plastic and rigid cells, bound together within segregated functional assemblies that support stable internal dynamics [23, 24]. Similarly, Purkinje cells (PC) are thought to constitute a scaffold for sequence learning in the cerebellum. Multiple developmental phases of climbing fiber synapse elimination targeting PC cells have been observed to build such a scaffold [15]. Similar phases of escalating development have been observed in the auditory cortex [17]. Conversely, these scaffolds are generally pruned in the final parts of development, yielding the emphasis to experience-dependent plasticity. This is clearly observed in cortex [25–27], where after initial development, synaptic formation, elimination, and modification are triggered by reciprocal neuronal activity. Initial geometrical connectivity therefore provides the potential for reconfigurations of local microcircuits.

These biological observations suggest a simplified model consisting of two phases of development and learning, with development creating a scaffold structure that is exploited and modified during learning (see Fig. 1 and discussion below). In the specific case of sequence learning, the neural network that emerges after the developmental process must support the stable representation of structured sequences of activity. Further, the network should make optimal use of available neuronal resources while the connectivity matrix should remain sparse to prevent exploding activity.

2.1 Early development provides a scaffold for learning

As an idealization of how such a network structure could emerge, we consider a stochastic model of cortical development for two neuronal populations of pyramidal neurons, an “output” population used for explicit representation of activity sequences and a “latent” population for storage and recall (Fig. 1a). These populations can be considered as corresponding to pre-motor (latent) and motor (output) areas. Our model first mimics a developmental phase that results in a scaffold of nudging connections which is later used for transporting target signals to the latent population during learning.

During this phase, somato-somatic connections are formed stochastically (Fig. 1b). Starting with the output population, each neuron that receives at least one somatic afferent forms a number n_{out} of efferent somato-somatic connections with decreasing probability $p^{n_{\text{out}}}$ (for details, see Sec. 5.2). These connections are then accepted by postsynaptic latent neuron partners with a decreasing probability $q^{n_{\text{in}}}$, where n_{in} represents the number of afferents they already have. During this phase, all neurons (from both output and latent populations) only project into the latent population. With appropriate choices of parameters p and q for the generating functions, this yields a homogeneously and sparsely connected network, where p controls the sparsity and q the uniformity. To model both excitation and inhibition, each somato-somatic connection is considered to consist of a direct excitatory connection

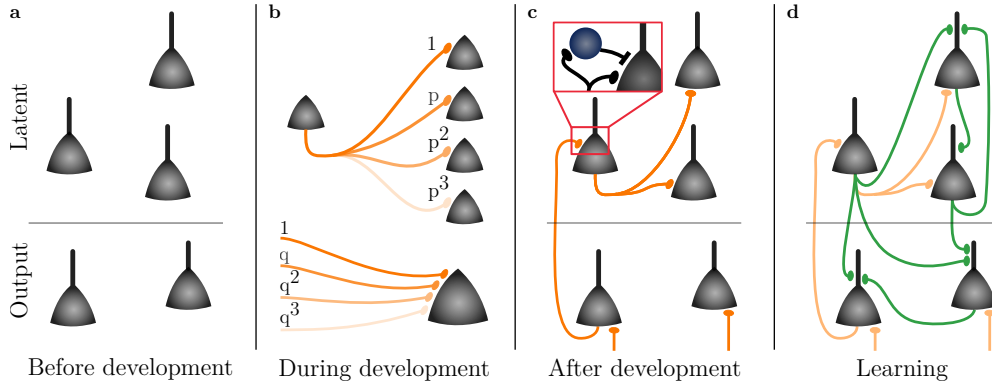


Figure 1: Development of somatic scaffold for the learning of dendritic connections. (a) The network composed of structured pyramidal neurons is divided into an output and latent population. (b) During development, axons (orange) extend to form a sparse scaffold of somato-somatic connections. Its structure is controlled by parameters p and q . (c) The connections of the somatic scaffold are static and have associated delays. Inhibition in the scaffold is mediated by interneurons. (d) Following development, somato-dendritic synapses (green) are learned according to a three-factor plasticity rule.

between the two neurons and additional inhibitory pathway via an interneuron (see Fig. 1c and Sec. 5.3). While we model all somato-somatic connections to be of equal strength, signals transmitted by different connections incur different, randomly drawn, transmission delays. Including delays emulates the characteristics of activity at the neuronal and sub-neuronal (axonal and dendritic) level, known to introduce temporal delays [28–30]. Similar treatments of delays are common in the modeling literature [31]. This network constitutes our starting point for learning, and can be seen as the scaffold which transports the teaching signal via “nudging”, i.e., transmitting target signals throughout the network that allow local plasticity to learn complex temporal sequences.

For modeling dendritic development, after the initial scaffolding phase, we set up weak all-to-all connections between somata and dendritic compartments of all neurons in both populations (Fig. 1d). During learning, only somato-dendritic synapses are plastic; the somato-somatic scaffold remains fixed after the initial developmental phase.

2.2 Neuronal dynamics and dendritic learning

We consider here a rate-based model in which both the somatic and the dendritic compartment are taken to be leaky integrators

$$C_m^{\text{den}} \dot{v} = -g_l (v - E_l) + I_{\text{syn}}^{\text{den}} \quad (1)$$

$$C_m^{\text{som}} \dot{u} = -g_l (u - E_l) + g_{\text{den}} (v - u) + I_{\text{syn}}^{\text{som}} \quad (2)$$

with v as the dendritic voltage, u the somatic voltage, C_m the compartmental capacitances, g_l the leak conductance, E_l the resting potential and g_{den} the coupling conductance between the dendritic and somatic compartments.

$I_{\text{syn}}^{\text{den}}$ and $I_{\text{syn}}^{\text{som}}$ represent the synaptic currents arriving at the dendritic compartment via the somato-dendritic connections and at the somatic compartment via the somato-somatic connections, respectively. The somatic compartment integrates the teaching input received via nudging and the input from the dendritic compartment. Synaptic input onto the dendritic compartment represents the driving force of neuronal activ-

ity and is modeled as current-based, to effectively account for signal propagation along the dendritic tree. Direct synaptic input to the soma is comparatively weak and conductance-based, thus only nudging neuronal activity into a particular direction. This type of neuronal compartmentalization, along with the interplay between driving and nudging synapses, has been shown to enhance the computational and learning capabilities of single neurons and the networks they form [20, 21, 32, 33]. For simplicity, we model the interaction between soma and dendritic tree as unidirectional (see also [32]). The firing rate r of a neuron is modeled as a logistic function of the somatic potential $r = \varphi(u)$, which also normalizes firing rates to the interval $[0, 1]$. For more details on the neuron and synapse models, we refer to Secs. 5.1 and 5.3.

In addition to providing a more realistic model for the spatial structure of biological neurons, our multi-compartmental setup also allows for the use of a local error-correcting learning rule (similar to [32]) for the somato-dendritic weights from neuron i to neuron j

$$\dot{w}_{ji}^{\text{den}} = \eta [\varphi(u_j) - \varphi(v_j^*)] \bar{r}_i \quad (3)$$

with a learning rate η and \bar{r} the low-pass filtered presynaptic rate. The weight updates minimize the difference between the somatic firing rate $\varphi(u)$, which is nudged towards a target behaviour by the somato-somatic connections, and the dendritic prediction of somatic firing $\varphi(v^*)$ (for additional details see Sec. 5.4). Learning modifies the synaptic weights of these connections, of which typically only a small proportion of stronger synapses become dominant, emulating dendritic pruning in biological brains. With this, the dendrite learns to drive the somatic voltage to produce the desired behavior as defined by the somato-somatic nudging. Learning converges once the latent population correctly drives the output neurons to reproduce the teacher activity. At this point the teaching signal can be removed without affecting the network activity.

In order for the network to learn, a teaching signal must be provided to the somatic compartment of the neurons in the output population. This signal nudges the somatic voltage of the output neurons towards the appropriate activation at

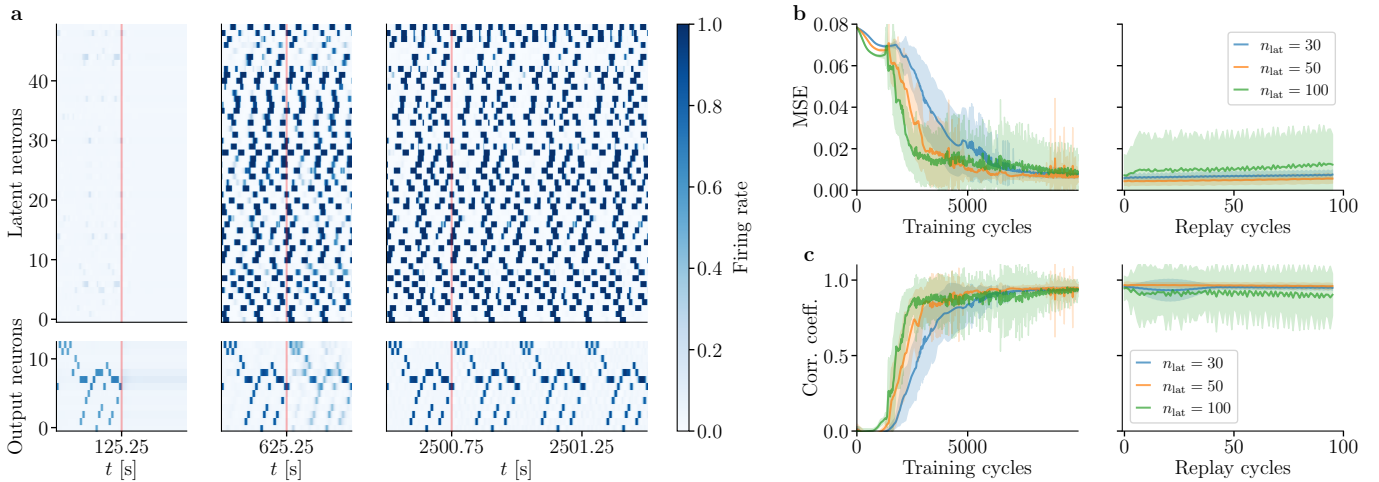


Figure 2: Learning process and replay ability of the network. (a) Evolution of network activity during learning. Output neurons are first nudged towards a particular target and then released in order to observe the network’s spontaneous activity (as demarcated by the red line). Snapshots during early (left), intermediate (middle) and final (right) stages of training. (b) Performance of networks with different latent population sizes measured by the mean squared error (MSE) loss between the activity of the output neurons and their target activity. Top: Evolution of the error during validation intervals, i.e. first replay of the pattern after being released from external nudging) during training. Bottom: Stability of replay after training, for continuous observation over many replay cycles following release from nudging. (c) Same as (b) but using the cross-correlation between output and target activities as a performance measure.

the appropriate times. timing. In turn, the somato-somatic connections distribute the teaching signal spatially and temporally (given the delays) towards the latent layer. Once the nudging is active, somato-dendritic connections learn to drive the dendritic voltage of postsynaptic partners towards the desired behavior.

3 Results

3.1 Local plasticity enables complex sequence replay

Following the developmental phase, the network can be trained to reproduce a complex spatio-temporal output sequence. Here, we train it to replay a long (compared to the neuronal time scales) non-Markovian pattern which serves as a mock-up of bird song. For this we chose the beginning phrase of Beethoven’s “Für Elise” (see Fig. 2). The output population contains 13 neurons, one for each different pitch in the musical phrase. The latent population contains 50 neurons for our baseline test. To train the network in the replay of the melody, the output population is repeatedly nudged towards a target activity pattern.

To observe the evolution of the network during learning, we interleave training with validation phases where the nudging to the output population is removed for one pattern duration and the free network activity is observed (Fig. 2a). This allows to compare the network activities in the nudged state with those in the free state and can be used to judge how well the network has already learned to replay the pattern on its own. As somato-dendritic synapses start out as weak, the activity in the latent layer is also too weak to sustain itself and the output activity without the nudging input. Learning then shapes and strengthens latent activity towards an increasingly structured and dynamical attractor that allows the network to keep replaying the sequence even when the teaching signal is

removed. For evaluating the quality of the pattern replay we use two measures: the MSE between the target pattern and the activity in the output population (Fig. 2b) and the correlation coefficient between the two (Fig. 2c). For a more detailed description of these performance measures, see the Methods Sec. 5.6. After training, a replay phase starts, in which nudging by the teacher is removed completely and the network is allowed to keep evolving in time. This evolution includes further weight plasticity, but in the absence of a teaching signal to the output population.

Our results in Fig. 2b and c show that latent populations as small as 30 neurons are sufficient to learn a very accurate and stable replay of the chosen output pattern. Importantly, as our model is capable of distributing useful teaching signals throughout the latent population, it can fulfill its task with a much smaller pool of neurons compared to other models of birdsong learning or reservoir computing [10, 11, 13, 34]. Furthermore, the high fidelity of the produced pattern over 100 replay episodes shows that the network does not unlearn even though it remains plastic during replay.

3.2 Learning of latent connectivity enables sustained pattern replay

To isolate and highlight the importance of learning in the latent population, we perform an ablation study. We compare our model containing plastic all-to-all somato-dendritic connections to a restricted version in which we only allow learning of the somato-dendritic weights that connect to the output population. Note that this ablated network is still more powerful than a standard reservoir, as it allows learning of recurrent connections in the output population; additional ablation of learning in these recurrent weights would recover the reservoir computing paradigm. Reservoirs and similar networks are known to be sensitive to the initialization of their latent weights [35–38]. Therefore, to ensure that we initialize our

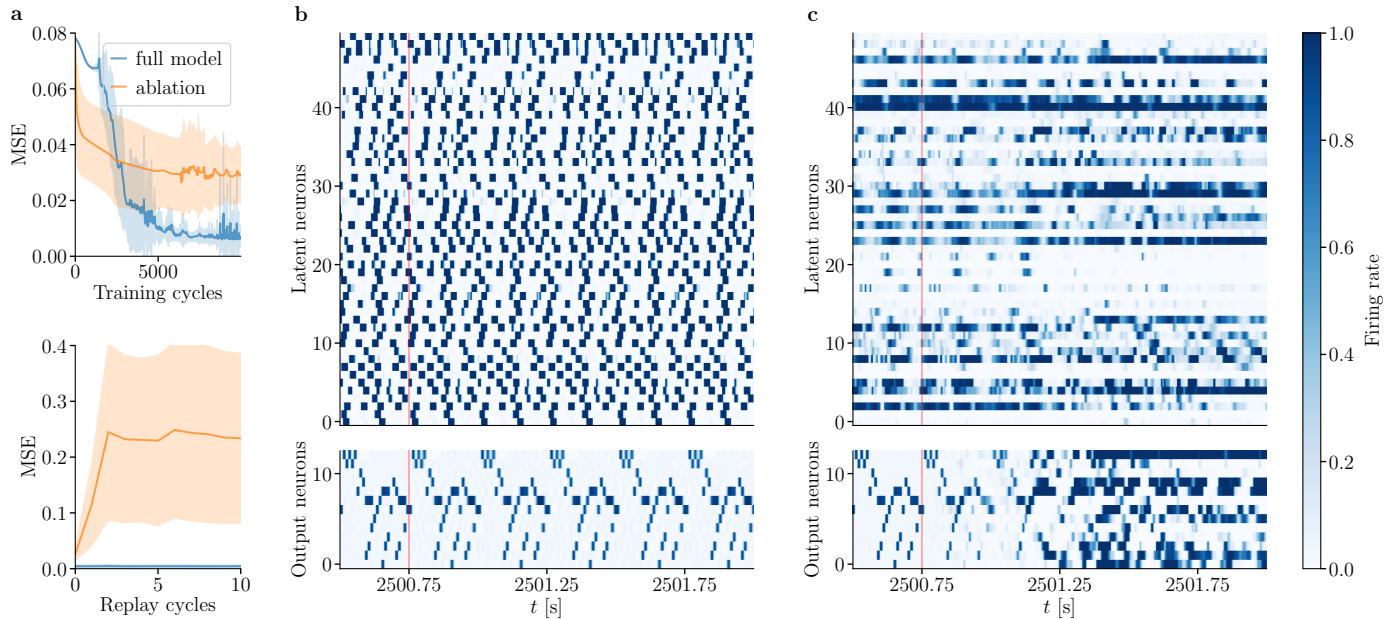


Figure 3: Comparison of replay performance between networks with and without learning of latent connections. (a) Accuracy and stability of sequence replay, measured by the MSE between generated and target activity. Top: MSE between target and produced pattern during training. Bottom: MSE during continued replay after training. (b) Recorded activity of the output (bottom) and latent (top) neurons of the fully plastic network during free replay of the pattern after training. The red line marks the end of the external input from the teacher. (c) Same as (b) but for the ablated network.

ablated networks in a way that does not prevent them from solving the task, we record the final weight distribution in the fully-trained (non-ablated) networks and initialize the static weights in the ablated networks with weights drawn randomly from that distribution. This fulfills the principle of random initialization of a reservoir, while at the same time simplifying the work of the reservoir, as the initial distribution of weights is known to be able to solve the problem.

Figure 3 shows that while the reservoir-mimicking ablated model seems to converge faster during training, the full model, capable of learning all connections, is able to reach a much lower replay errors. The observed increase in convergence speed is a direct consequence of having already initialized the latent weights in a useful regime for the specific task to be solved. In contrast, the full model starts with vanishing latent weights which need to be learned in the first place. However, training speed is obviously irrelevant if the network ultimately fails to perform the sought task. As seen in Figure 3c, while the full model is capable of self-sustained replay of the target pattern, the ablated network quickly diverges from the target pattern following the removal of the teacher.

3.3 Learning engenders robustness to internal variability and external disruption

Aside from raw performance, we consider robustness to be an essential property of biologically plausible models. The requirement of finely tuned parameters or disturbance-free operation is difficult to reconcile with the conditions under which biological neural networks must operate.

First, we demonstrate that our model is capable of accurate and stable sequence learning over a wide parameter range of p

and q , which control the developmental process and hence the connectivity of the nudging scaffold (Fig. 4a and b). Next, we study the impact of a less dense somato-dendritic connectivity (Fig. 4c and d) by changing the proportion r of non-zero and learnable connections (for more information about the sparsity see Methods Sec. 5.5.2). While sparser networks require more training cycles to learn, networks with only 40% of all available connections are still able to learn and replay the pattern with low error (Fig. 4c). Furthermore, we find that learning in even sparser networks is possible if we ensure that the somato-dendritic connections that follow the scaffold of nudging connections remain non-zero (Fig. 4d). Since it is this somato-somato scaffold that propagates the teaching signals throughout the network, it appears plausible that the somato-dendritic connections that follow this scaffold are especially important for learning the task.

To model the effect of external disruptions to the output population activity, we temporarily clamp the somatic voltages of the output neurons to fixed values (Fig. 5, see Methods Sec. 5.5.1 for details). Although limited to the output layer, this can represent a strong disruption, as the output layer plays a central role during learning, and clamping these neurons necessarily disturbs the behavior of the entire network. For maximal impact, we clamp the voltage of the output neurons either to their leak potential, modeling strong external suppression (Fig. 5a and b), or to a high voltage above the leak potential, modeling strong external excitation (Fig. 5c and d). In both cases the network activity recovers (in all trials if only part of the pattern is disrupted and in most trials even when disrupting the entire pattern for one cycle) following a short transient phase during which the network settles back into its original behavior (see also Supplementary Figure 7). These experiments show that the dynamical attractors carved into

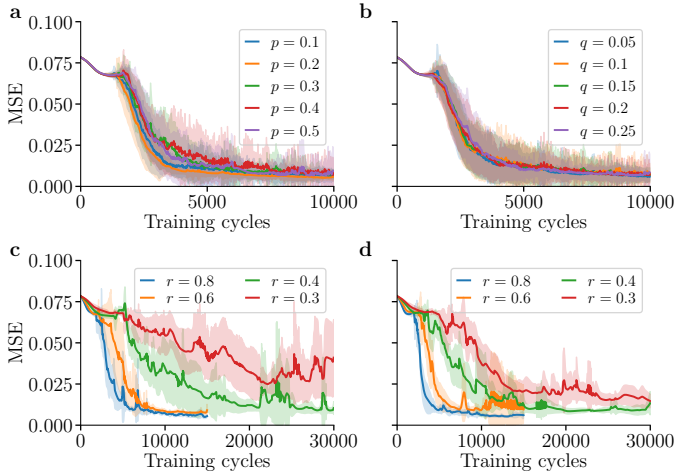


Figure 4: Robustness of learning with respect to changes in the network parameters. (a) Sweep over network parameter p . For each p runs with a range of q values and multiple seeds are averaged. (b) Sweep over network parameter q . For each q runs with a range of p values and multiple seeds are averaged. (c) Training of networks with sparse somato-dendritic connectivity; r represents the proportion of nonzero and plastic synapses out of all possible somato-dendritic connections in the network. (d) Same as (c) but the somato-dendritic connections that match an already existing somato-somatic connection are protected from sparsification.

the networks’ phase space by the dendritic learning are strong enough to withstand considerable disruptions.

4 Discussion

In this work we describe ELiSe, an efficient and biologically plausible model of complex spatio-temporal sequence learning. We take inspiration from biology in two ways. First, we model structured neurons composed of a dendritic and a somatic compartment. This allows synapses local access to multiple factors required for learning [32]. Second, we introduce structure to the network connectivity prior to learning, in a process mimicking early development. Intuitively this propagates teaching signals (targets) throughout the network in a structured way, unlike in a randomly initialized network with dense connectivity. This allows postsynaptic neurons to select those presynaptic partners that generate useful activity at the right moment in time. We show that networks trained with ELiSe are able to learn and then replay complex non-Markovian sequences to a high accuracy while remaining extremely parsimonious in their use of neuronal resources. By comparing our model to a reservoir-like ablation, we show that plasticity in the latent connections is crucial for replay, as it carves out specific stable dynamical attractors in the space of latent neuron activities. ELiSe further improves upon reservoir computing models as it is not sensitive to initial conditions and does not require fine-tuning of hyper-parameters [35–38].

4.1 Comparison to other approaches

ELiSe compares favorably to other models of biologically plausible sequence learning. Most notably, in comparison to others of its kind, our model is very resource efficient. Requiring as little as 30 hidden neurons to learn a long non-Markovian se-

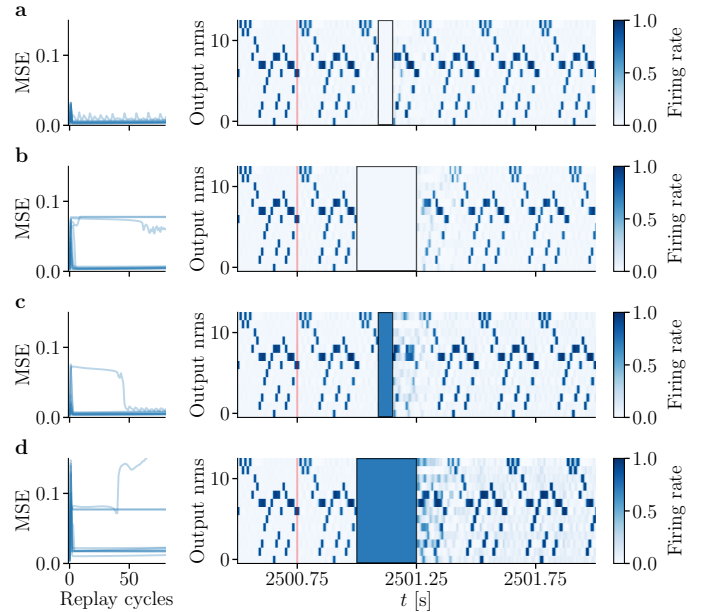


Figure 5: Network replay is robust to strong disruptions of its output activity. (a) Left: MSE for 10 different networks during disturbed pattern replay. Right: Activity in the output population during pattern replay (red line marks end of teacher nudging). During the second replay pattern output activity is suppressed (black box) by clamping the membrane voltages of all output neurons. (b) Same as (a) but with a disturbance for the duration of a whole pattern. (c) Short disturbance but instead of suppressing neuron activity, “wrong” activity is introduced into the network by clamping to a high membrane voltage. (d) Same as (c) but with a disturbance for the duration of a whole pattern.

quence, it uses at least an order of magnitude fewer neurons than comparable biological sequence learning models (FORCE [10], FOLLOW [12], the “clock chain” approach by [13] and a spiking hierarchical temporal memory (HTM) [39]). As discussed above, we suggest that the main reason lies in the structured propagation of learning signals in ELiSe. In our model this propagation is performed very efficiently via sparse, delayed somato-somatic connections. This use of delays is not plausible in models where learning relies either on instantaneous error signals (FORCE, FOLLOW) or propagated errors (RTRL [8], RFLO [9]). Thus these models rely solely on the slow neuron dynamics and network size to create the required transients. While the spiking HTM makes use of delays, this is only done to restrict learning between proximal neurons.

Further, our model is structurally simple. The only distinguishing feature between the two populations (latent and output) is that the former receives an external teaching input. In contrast, other models of learning in recurrent networks (FORCE, FOLLOW) make use of distinct functional units, such as for computing and transporting errors and signals, coupled with strong assumptions about the resulting connectivity. For example [10, 12] makes use of precise error computation in output neurons that project to all neurons in the recurrent population. The architectural simplicity of ELiSe is complemented by the simplicity and uniformity of its associated plasticity rule. Most importantly, it is fully local and does not require the use of a global error signal [10, 12]. Finally, it does not require different phases [12] nor does it make biologically

implausible assumptions about learning speed [10].

4.2 Neural correlates

While we do not model cortical areas explicitly, we can draw parallels between brain areas and their suggested functional roles and the components and dynamics of our model. Here we compare our model to the neural mechanisms underlying birdsong learning in Zebra finches; much like ELiSe, these birds learn a single song based on that of their teacher. [40, 41]. In our model learning structures the latent activity until it becomes almost identical across replays of the sequence. Qualitatively, this matches observations in zebra finches that during learning the activity in pre-motor area RA becomes increasingly self-similar [1, 42, 43]. Furthermore, in our model the teaching signal is already structured at the onset of learning owing the somato-somatic scaffold established during early development. Similarly, evidence suggests that songbirds are born with a species-specific template that is refined through listening to the tutor [44–46]. Indeed, once the bird has learned the crystallized adult song, the removal of areas encoding the song (caudomedial nidopallium, caudomedial mesopallium) caused impairment of the tutor song recognition but not replay [45]. Likewise, once our model has learned the sequence, the somato-dendritic connections no longer contribute to sequence replay and could be removed.

Finally, both our model and birdsong learning leverage sources of random unstructured activity to improve learning. In our model the randomly initialized somato-dendritic connections initially propagate activity in a weak and unstructured way. Learning allows ELiSe to single out and strengthen those connections that contribute to correct replay. In birdsong learning variability is provided to pre-motor area RA by the lateral magnocellular nucleus of the anterior nidopallium (LMAN) [47, 48]. It has been suggested that when variable LMAN activity contributes to song replay, subcortical structures encoding reward signals induce plasticity in connections which then bias LMAN towards producing useful activity in the future [49, 50]. These analogies between songbird learning and our model suggest that the interplay of structure and randomness is an essential feature of sequence learning systems.

4.3 Open questions and future work

Our model makes several simplifications, which we discuss in the following.

First, it does not explicitly obey Dale’s law for the somato-dendritic synapses, simultaneously allowing both excitatory and inhibitory efferent connections. However, the somato-somatic interaction between pairs of pyramidal cells always follows a dual pathway, one direct and one mediated by an inhibitory interneuron. While important for controlling the duration of this interaction [51, 52], the same mechanism can also be leveraged to implement a net inhibitory effect of somato-dendritic interactions, as well as a seamless transition between net excitation and inhibition if plasticity is present in both pathways. The implicitly assumed statistical balance between excitation and inhibition is supported by theoretical and ex-

perimental findings [53–56]

Second, we use rate-based neurons and forego the explicit modeling of spikes. However, we expect ELiSe to transfer seamlessly to the spike-based regime. The activity in our latent layer is strongly reminiscent of synfire braids and polychronization in spiking networks [31, 57–59]. Moreover, our specific arrangement with paired feedforward inhibition exhibits the particularly appealing feature of convergence towards stable propagation [60], with particular robustness towards variability in the neuronal substrate [61, 62].

We believe this work inspires three further avenues of research. First, the full computational performance of ELiSe is yet to be explored. For example, here we are focussing on learning a single non-Markovian sequence. However, we expect our setup to also be applicable in scenarios with multiple patterns. This would require larger networks and a training procedure that teaches the network all patterns at the same time, to prevent catastrophic forgetting. Second, it would be interesting to investigate more closely the link to the biological correlates of sequence learning. One approach could be to explicitly model the functional properties of neuronal populations involved in sequence learning. For example, one could investigate how the explicit inclusion of an external area providing random input (like LMAN) or clock like input (like HVC) would affect learning in the model. Alternatively, one could compare how our model networks and biological brains respond to the same kinds of disruptions such as cutting certain connections, injecting external currents or optogenetically activating individual populations. Finally, we believe that the inherent resource efficiency, locality and robustness to disturbances make ELiSe an interesting candidate for deployment on neuromorphic systems and small-scale robotic platforms. Especially in energy-constrained environments, for example on a small robotic system with a fixed motor activation sequence for movement, the small but also resilient network architectures learnt by ELiSe could provide tangible benefits compared to commonly deployed solutions.

5 Methods

5.1 Neuron model

We model our neurons as two compartments (a somatic and a dendritic one) which are both leaky integrators. The compartments are coupled with a conductance g_{den} but only the dendrite influences the soma and not the other way around. The dendritic membrane voltage v is described as

$$C_m^{\text{den}} \dot{v} = -g_l (v - E_l) + I_{\text{syn}}^{\text{den}} \quad (4)$$

where C_m^{den} is the capacitance of the dendritic compartment, g_l is its leak conductance and E_l the resting potential. The synaptic currents invoked by the incoming somato-dendritic connections are subsumed in $I_{\text{syn}}^{\text{den}}$. The somatic membrane voltage u is modeled as

$$C_m^{\text{som}} \dot{u} = -g_l (u - E_l) + g_{\text{den}} (v - u) + I_{\text{syn}}^{\text{som}} \quad (5)$$

where C_m^{som} is the capacitance of the somatic compartment, g_l is its leak conductance, E_l the resting potential and g_{den} is the conductance coupling the dendrite to the soma. The synaptic currents invoked by the incoming somato-somatic connections are subsumed in $I_{\text{syn}}^{\text{som}}$. The firing rate r of the neuron is a logistic function of the somatic voltage

$$r = \varphi(u) = \frac{1}{1 + \exp(a(b - u))} \quad (6)$$

with parameters $a = 0.3$ and $b = -58$. All additional parameters can be found in Table 1 in the supplementary materials in the Supplement Table 1.

5.2 Developmental setup

In order to mimic biological developmental processes, we use a stochastic algorithm that relies only on local information. We start out with two populations of neurons that have no synaptic connections, a latent and an output population. Each neuron in the output population receives a somatic nudging connection from a teacher. From this starting scenario we run a stochastic iterative algorithm to form the scaffold of somato-somatic connections.

The algorithm generates outgoing nudging (somato-somatic) connections for those neurons which have at least one incoming nudging connection. This ensures that only those neurons receiving teaching input themselves teach others. Initially the only neurons with incoming nudging connections are those in the output layer. During the wiring process, one neuron i is randomly chosen from the set of neurons that receive nudging inputs and have not yet formed any outgoing connections. This neuron i makes X ($X \geq 0$) outgoing nudging connections. The probability to form zero connections is p_0 , with a default of $p_0 = 0.04$. For $X > 0$, the first outgoing connection is made with probability $1 - p_0$. Afterwards, the neuron develops additional outgoing connections with probability $p^{n_{\text{out}}}$. Here, $p = 0.2$ by default and n_{out} is the number of already existing outgoing connections. Note, this is an iterative process, once the check if n connections should be made succeeded, a new random number is drawn and the check for $n+1$ connections is performed. Hence, the probability of $X = k$ is (see Figure 6):

$$P(X = k) = \begin{cases} p_0 & \text{if } k = 0 \\ (1 - p_0)p^{\frac{k^2 - k}{2}}(1 - p^k) & \text{if } k \geq 1 \end{cases} \quad (7)$$

To find post-synaptic partners for the X connections, for each for the X connections a neuron j from the latent population is selected randomly. In the case that $i = j$ a new neuron is drawn as self-nudging is not possible. Otherwise the probability for that neuron j accepts the incoming connection is q^M where M is the number of previously accepted incoming connections (default: $q = 0.15$). Therefore, a neuron that does not have incoming connections yet, will always accept its first connection. If neuron j rejects the connection, a new random neuron is selected. Once a neuron j accepts the connection, it is added to the set of neurons that must form outgoing connections, if it is not already in there. When all X connections are

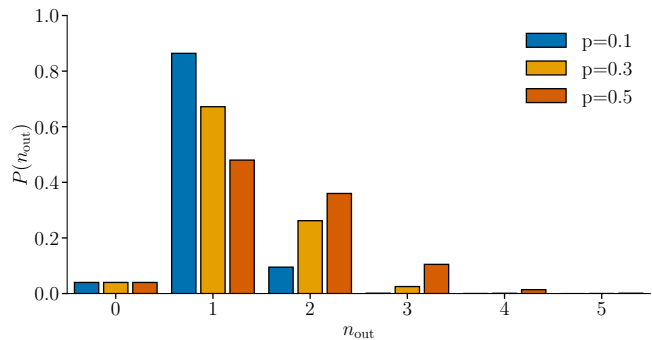


Figure 6: Distribution of $P(n_{\text{out}})$. Probability distribution of the number of outgoing connections n_{out} formed by a neuron depending on the parameter p . It can be described as a second order non-homogenous geometric distribution which is sparser than a first-order homogenous one.

formed, neuron i is permanently removed from the set of neurons that form outgoing connections, a new i is chosen and the process repeats. The setup algorithm terminates once there are no more neurons left in the set of neurons wanting to form outgoing connections. Intuitively, we can think of p controlling the density and q the uniformity of the scaffold.

After the setup of the somato-somatic nudging scaffold, the somato-dendritic connections are initialized as an all-to-all (including output and latent population) weight matrix. The individual weight values are drawn from a Gaussian distribution with configurable means and standard deviations. In particular, means and standard deviations can be set to different values for the 4 different subsets of connections: from output to latent, from output to output, from latent to latent and from latent to output. By default, the mean is at zero and $\sigma = 0.5$. For the experiments with sparse dendritic connections, the whole all-to-all weight matrix exists, but some of the connection weights are clamped to zero.

5.3 Synaptic connections

There are two types of synaptic connections: the conductance-based somato-somatic (“nudging”) connections and the current-based somato-dendritic connections.

5.3.1 Somato-dendritic connections

The dendritic connection from neuron i to neuron j is characterized by its synaptic weight w_{ji}^{den} and its transmission delay d_{ji}^{den} . All dendritic connections originating from neuron i share the same d_i^{den} as a model for the delay introduced by the length of the axon. The values of the dendritic delays are determined at network initialization and are multiples of the simulation time step ($dt = 0.1$ ms). They are drawn from a uniform distribution between $[d_{\text{min}}^{\text{den}}, d_{\text{max}}^{\text{den}}]$ with $d_{\text{min}}^{\text{den}} = 5$ ms and $d_{\text{max}}^{\text{den}} = 15$ ms in our simulations. The summed synaptic current onto the dendritic compartment of neuron j is then

$$I_{\text{syn},j}^{\text{den}}(t) = \sum_i w_{ji}^{\text{den}} r_i(t - d_i^{\text{den}}) \quad (8)$$

with r_i representing the presynaptic firing rate.

5.3.2 Somato-somatic connections

The nudging scaffold consists of sparse, conductance-based somato-somatic connections. If the developmental algorithm in Sec. 5.2 sets up a nudging connection from neuron i to neuron j , this nudging connection consists of an excitatory and an inhibitory connection. The inhibitory connection is assumed to be produced via an inhibitory interneuron which is not explicitly modeled here (see Fig. 1c). Due to this “additional length in signal transmission path” the inhibitory connection is assumed to have a larger delay than its corresponding excitatory one. This is modeled by the transmission delay $d_{\text{inh},i}^{\text{som}}$ always being larger by a fixed amount δ $d_{\text{inh},i}^{\text{som}} = d_{\text{exc},i}^{\text{som}} + \delta$. In our case $\delta = 25$ ms. The delay of all excitatory outgoing nudging connections formed by a neuron i $d_{\text{exc},i}^{\text{som}}$ is a multiple of the simulation time step Δt and is drawn from a uniform distribution between $[d_{\text{min}}^{\text{som}}, d_{\text{max}}^{\text{som}}]$ with $d_{\text{min}}^{\text{som}} = 5$ ms and $d_{\text{max}}^{\text{som}} = 15$ ms in our simulations. All nudging connections have the same strength, so we omit their synaptic weight here by implicitly setting it to 1 for all nudging connections. The summed synaptic current onto the somatic compartment of neuron j is

$$I_{\text{syn},j}^{\text{som}}(t) = \sum_i [g_{\text{exc},i}(t)(E_{\text{exc}} - u) + g_{\text{inh},i}(t)(E_{\text{inh}} - u)] \quad (9)$$

where E_{exc} and E_{inh} are the excitatory and inhibitory reversal potential. The synaptic conductances $g_{\text{exc},i}(t)$ and $g_{\text{inh},i}(t)$ depend on the (delayed) firing rate r_i of the pre-synaptic neuron i :

$$g_{\text{exc},i}(t) = \begin{cases} g_{\text{exc},0} r_i(t - d_{\text{exc},i}^{\text{som}}) & \text{if } r_i(t - d_{\text{exc},i}^{\text{som}}) > \varphi(E_1) \\ g_{\text{exc},0} \varphi(E_1) & \text{otherwise} \end{cases} \quad (10)$$

$$g_{\text{inh},i}(t) = \begin{cases} g_{\text{inh},0} r_i(t - d_{\text{inh},i}^{\text{som}}) & \text{if } r_i(t - d_{\text{inh},i}^{\text{som}}) < \varphi(E_1) \\ g_{\text{inh},0} \varphi(E_1) & \text{otherwise} \end{cases} \quad (11)$$

In the case where the nudging (i.e. the teacher) is removed for the output neurons (typically during replay) the conductances g_{exc} and g_{inh} are set to zero.

5.3.3 Teaching synapses

The output neurons receive their somatic inputs from an external teacher. While the synaptic current $I_{\text{syn}}^{\text{som}}$ induced by these teaching synapses is of the same form as described in Eq. (9), the values of $g_{\text{exc}}(t)$ and $g_{\text{inh}}(t)$ are determined (without any delay) by the target pattern:

The target pattern consists of an array of values between 0 and 1 for each output neuron, which indicates the activity over the pattern duration (a 0 indicating minimal firing rate and a 1 indicating maximal firing rate). In our example the pattern consists exclusively of the discrete values of 0 and 1 but in principle intermediate target activities are possible. The target activities are mapped to target voltages $u_{\text{tgt}}(t)$ and we choose to map a target activity of 0 to E_1 and 1 to $E_1 + 20$.

For a neuron model as described in Secs. 5.1 and 5.3 we know from [32] that if the somatic potential is equal to a so-called

“matching potential”

$$u_M = \frac{g_{\text{exc}} E_{\text{exc}} + g_{\text{inh}} E_{\text{inh}}}{g_{\text{exc}} + g_{\text{inh}}}, \quad (12)$$

then the net-effect of the conductance-based synapses to the soma amounts to zero and the somatic voltage u tend towards the same value, even if the somatic connections are removed. This is exactly the behavior we want from our teaching synapses: Once the somatic voltage reaches its target, we want to be able to take the teaching synapses away and the neuron should still be able to produce the same (target) somatic voltage. Therefore, the target voltage for the output neurons u_{tgt} must correspond to the matching potential u_M induced by the conductance based teaching synapses. From this we can calculate the resulting synaptic conductances g_{exc} and g_{inh} that produce the desired matching potential by setting

$$u_{\text{tgt}} = \frac{g_{\text{exc}} E_{\text{exc}} + g_{\text{inh}} E_{\text{inh}}}{g_{\text{exc}} + g_{\text{inh}}} \quad (13)$$

and solving for the conductances:

$$g_{\text{exc}} = \frac{g_{\text{inh}}(E_{\text{inh}} - u_{\text{tgt}})}{u_{\text{tgt}} - E_{\text{exc}}} \quad (14)$$

$$g_{\text{inh}} = \frac{g_{\text{exc}}(u_{\text{tgt}} - E_{\text{exc}})}{E_{\text{inh}} - u_{\text{tgt}}} \quad (15)$$

As this is underdetermined, we impose another condition that enables us to balance the strength of the teacher nudging with the strength of leak and dendritic compartment by setting

$$g_{\text{exc}} + g_{\text{inh}} = \frac{\lambda}{1 - \lambda} (g_1 + g_{\text{den}}) \quad (16)$$

with λ as a scaling parameter that we typically set to $\lambda = 0.6$. From this we can calculate the conductances of the teaching synapses dependent on the target voltage u_{tgt} given by the target pattern:

$$g_{\text{exc}}(u_{\text{tgt}}) = \frac{\lambda}{1 - \lambda} (g_1 + g_{\text{den}}) \frac{(E_{\text{inh}} - u_{\text{tgt}})}{E_{\text{inh}} - E_{\text{exc}}} \quad (17)$$

$$g_{\text{inh}}(u_{\text{tgt}}) = \frac{\lambda}{1 - \lambda} (g_1 + g_{\text{den}}) \frac{(u_{\text{tgt}} - E_{\text{exc}})}{E_{\text{inh}} - E_{\text{exc}}} \quad (18)$$

5.4 Plasticity

Only the somato-dendritic synapses are plastic. They learn with a local error-correcting learning rule similar to [32]:

$$\dot{w}_{ji}^{\text{den}} = \eta [\varphi(u_j) - \varphi(v_j^*)] \bar{r}_i \quad (19)$$

where η is the learning rate and is different for the connections among the output neurons (η_o) and all other connections (η_l). v^* is a scaled version of the dendritic voltage that corresponds to the voltage in the soma that a dendritic potential v would elicit if the soma did not receive any additional input:

$$v^* = \frac{1}{g_1 + g_{\text{den}}} [g_1 E_1 + g_{\text{den}} v] \quad (20)$$

\bar{r} is a low-pass filter of the delayed pre-synaptic rate r_i and represents the impact of the pre-synaptic rate on the dendritic

potential

$$\dot{\tilde{r}}_i(t) = -g_1 \tilde{r}_i(t) + \frac{g_1 g_{\text{den}}}{g_1 + g_{\text{den}}} r_i(t - d_i^{\text{den}}). \quad (21)$$

5.5 Training setup

The network is trained by repeatedly nudging the output neurons towards the target pattern. Typically the target is presented for 10000 cycles, with the exception of the sparsity experiments which required longer training times. There is no reset of voltages or rates between the cycles. Interleaved into the training cycles, typically at intervals of 20 training cycles, there is one replay cycle to quantify training progress. For these interleaved “validation” cycles the teacher nudging of the output neurons is removed. Weight updates continue during these validation cycles.

After the training cycles are completed, the replay phase, typically 100 cycles, starts. There is no reset of voltages or rates at the switch between training and replay. During the first three replay cycles the nudging is still active. Afterwards it is switched off and the network activity evolves without any outside influence. Learning is always on during the replay phase, but since the nudging of the output neurons is off, the weights do not change strongly. We keep the learning switched on to demonstrate that the system, if left alone, does not unlearn.

5.5.1 Disruptions

For the experiments shown in Fig. 5 the activity of the neurons in the output population is disturbed during the replay phase. This is achieved by clamping the somatic voltage of the disrupted neurons to a fixed value $u(t) = u_{\text{disrupt}}$ for all times t within a given interval. Both the disturbance interval duration and the voltage neurons are clamped to are varied in the shown experiments. To model a disruption that silences the output neurons $u_{\text{disrupt}} = E_1$ is chosen. Conversely, to mimic a disruption that makes the output neurons produce strong “wrong” activity we set $u_{\text{disrupt}} = E_1 + 15$.

5.5.2 Sparsity

The experiments in Fig. 4 c and d investigate the impact of sparser somato-dendritic connectivities. At the initialization of the somato-dendritic weight matrix, each entry is set to zero with the probability of $1 - r$, with r being the chosen connection density of the somato-dendritic connections. For Fig. 4d we protect those pairs of pre- and post-synaptic neurons from having their somato-dendritic weight nullified that also have a somato-somatic connection.

5.6 Performance measures

There are several possible measures to compare the similarity of the temporal sequence produced by the output population and the target sequence. We use both the MSE and the correlation coefficient Coeff. The correlation coefficient, specifically the Pearson correlation coefficient, is defined as the normalized

covariance cov between two signals x and y :

$$\text{Coeff} = \frac{1}{\sqrt{\text{cov}(x, x)\text{cov}(y, y)}} \text{cov}(x, y) \quad (22)$$

In our case the signals $x = [x_0, x_1, \dots, x_T]$ is the output rate of an output neuron over time and y the target for this neuron. The covariance is defined as

$$\text{cov}(x, y) = \frac{1}{T} \sum_{t=0}^T (x_t - E[x]) (y_t - E[y]) \quad (23)$$

where $E[x]$ is the expectation value of the variable x and $E[y]$ the expectation value of y . We then average the Coeff for all output neurons to get the final performance score. While the correlation coefficient has the advantage of having easily interpretable performance values (a score of 1 being the optimum), a major disadvantage of it is that it is insensitive to a downscaling of the signal, e.g. $\text{Coeff}(x, y) = \text{Coeff}(\frac{1}{10}x, y)$.

We therefore complement it with the MSE as an additional performance measure. The MSE for each neuron is calculated as mean over the quadratic differences between output rate and target for every time step:

$$\text{MSE}(x, y) = \frac{1}{T} \sum_{t=0}^T (x_t - y_t)^2 \quad (24)$$

We then average the MSE of all output neurons. The advantage of this measure is that it is sensitive to a scaling of one of the signals, therefore e.g. a weakening of the output during replay can be detected. However interpreting the performance values is slightly more unintuitive, because while it is clear that lower is better, the absolute values of the MSE are not directly meaningful.

The combination of two different performance measures of which one is sensitive and one insensitive to a scaling of signals is advantageous because it provides more insights into the networks behavior and gives hints to reasons for performance losses. If there is, for example, a dip in performance during replay that is visible in only the scaling-sensitive measure but not in the other one, this hints to a weakening of the signal because of loss of activity in the network. If however the dip is visible in both measures, then the performance loss must be caused by something else, i.e. a real decorrelation of the signal and the target.

5.6.1 Time shifts in the output signal

During replay the output pattern shifts slightly to later times with every repetition. We need to take this into account when evaluating replay performance. To evaluate replay performance we evaluate the performance for each pattern repetition separately, i.e. we calculate e.g. $\text{MSE}(x, y)$ with x and y containing the amount of time steps of one pattern duration T . For every replay repetition r we calculate the performance p_r by evaluating all possible pattern shifts s (not more than one

pattern length is allowed as shift) and taking the best one

$$p_r = \min_{s \in [0, T)} (\text{MSE}(x_{r,s}, y)) \quad \text{with} \quad (25)$$

$$x_{r,s} = x[rT + s, (r + 1)T + s] \quad (26)$$

where x is the full recording of the output over all replay repetitions, y is the target sequence, r the replay index, s the applied shift and T the pattern duration. Due to the shift, the quality of the last replay repetition can not be evaluated.

References

- [1] R. H. Hahnloser, A. A. Kozhevnikov, and M. S. Fee. “An ultra-sparse code underlies the generation of neural sequences in a songbird”. In: *Nature* 419.6902 (2002), pp. 65–70.
- [2] A. Leonardo and M. S. Fee. “Ensemble coding of vocal control in birdsong”. In: *Journal of Neuroscience* 25.3 (2005), pp. 652–661.
- [3] A. J. Peters, S. X. Chen, and T. Komiyama. “Emergence of reproducible spatiotemporal activity during motor learning”. In: *Nature* 510.7504 (2014), pp. 263–267.
- [4] A. Adler et al. “Somatostatin-expressing interneurons enable and maintain learning-dependent sequential activation of pyramidal neurons”. In: *Neuron* 102.1 (2019), pp. 202–216.
- [5] C. D. Harvey, P. Coen, and D. W. Tank. “Choice-specific sequences in parietal cortex during a virtual-navigation decision task”. In: *Nature* 484.7392 (2012), pp. 62–68.
- [6] M. Lukoševičius and H. Jaeger. “Reservoir computing approaches to recurrent neural network training”. In: *Computer Science Review* 3.3 (2009), pp. 127–149.
- [7] P. J. Werbos. “Backpropagation through time: what it does and how to do it”. In: *Proceedings of the IEEE* 78.10 (1990), pp. 1550–1560.
- [8] D. Zipser. “A subgrouping strategy that reduces complexity and speeds up learning in recurrent networks”. In: *Neural Computation* 1.4 (1989), pp. 552–558.
- [9] J. M. Murray. “Local online learning in recurrent networks with random feedback”. In: *eLife* 8 (2019), e43299.
- [10] D. Sussillo and L. F. Abbott. “Generating coherent patterns of activity from chaotic neural networks”. In: *Neuron* 63.4 (2009), pp. 544–557.
- [11] W. Nicola and C. Clopath. “Supervised learning in spiking neural networks with FORCE training”. In: *Nature Communications* 8.1 (2017), p. 2208.
- [12] A. Gilra and W. Gerstner. “Predicting non-linear dynamics by stable local learning in a recurrent spiking neural network”. In: *eLife* 6 (2017), e28295.
- [13] A. Maes, M. Barahona, and C. Clopath. “Learning spatiotemporal signals using a recurrent spiking network that discretizes time”. In: *PLoS Computational Biology* 16.1 (2020), e1007606.
- [14] A. M. Zador. “A critique of pure learning and what artificial neural networks can learn from animal brains”. In: *Nature Communications* 10.1 (2019), p. 3770.
- [15] M. Kano et al. “Multiple phases of climbing fiber synapse elimination in the developing cerebellum”. In: *The Cerebellum* 17 (2018), pp. 722–734.
- [16] R. Cossart and R. Khazipov. “How development sculpts hippocampal circuits and function”. In: *Physiological Reviews* 102.1 (2022), pp. 343–378.
- [17] M. Chang and P. O. Kanold. “Development of auditory cortex circuits”. In: *Journal of the Association for Research in Otolaryngology* 22.3 (2021), pp. 237–259.
- [18] M. Larkum. “A cellular mechanism for cortical associations: an organizing principle for the cerebral cortex”. In: *Trends in Neurosciences* 36.3 (2013), pp. 141–151.
- [19] G. Stuart, N. Spruston, and M. Häusser. *Dendrites*. Oxford University Press, 2016.
- [20] M. London and M. Häusser. “Dendritic computation”. In: *Annual Review of Neuroscience* 28 (2005), pp. 503–532.
- [21] P. Poirazi and A. Papoutsi. “Illuminating dendritic function with computational models”. In: *Nature Reviews Neuroscience* 21.6 (2020), pp. 303–321.
- [22] A. Payeur, J.-C. Béique, and R. Naud. “Classes of dendritic information processing”. In: *Current Opinion in Neurobiology* 58 (2019), pp. 78–85.
- [23] A. D. Grosmark and G. Buzsáki. “Diversity in neural firing dynamics supports both rigid and learned hippocampal sequences”. In: *Science* 351.6280 (2016), pp. 1440–1443.
- [24] A. Malvache et al. “Awake hippocampal reactivations project onto orthogonal neuronal assemblies”. In: *Science* 353.6305 (2016), pp. 1280–1283.
- [25] D. B. Chklovskii, B. Mel, and K. Svoboda. “Cortical rewiring and information storage”. In: *Nature* 431.7010 (2004), pp. 782–788.
- [26] N. Kalisman, G. Silberberg, and H. Markram. “The neocortical microcircuit as a tabula rasa”. In: *Proceedings of the National Academy of Sciences* 102.3 (2005), pp. 880–885.
- [27] J.-V. Le Bé and H. Markram. “Spontaneous and evoked synaptic rewiring in the neonatal neocortex”. In: *Proceedings of the National Academy of Sciences* 103.35 (2006), pp. 13214–13219.
- [28] K. K. Sreenivasan and M. D’Esposito. “The what, where and how of delay activity”. In: *Nature Reviews Neuroscience* 20.8 (2019), pp. 466–481.
- [29] D. J. Bakkum et al. “Tracking axonal action potential propagation on a high-density microelectrode array across hundreds of sites”. In: *Nature Communications* 4.1 (2013), p. 2181.

- [30] J. Zylberberg and B. W. Strowbridge. “Mechanisms of persistent activity in cortical circuits: possible neural substrates for working memory”. In: *Annual Review of Neuroscience* 40.1 (2017), pp. 603–627.
- [31] E. M. Izhikevich. “Polychronization: computation with spikes”. In: *Neural Computation* 18.2 (2006), pp. 245–282.
- [32] R. Urbanczik and W. Senn. “Learning by the dendritic prediction of somatic spiking”. In: *Neuron* 81.3 (2014), pp. 521–528.
- [33] J. Sacramento et al. “Dendritic cortical microcircuits approximate the backpropagation algorithm”. In: *Advances in Neural Information Processing Systems* 31 (2018).
- [34] H. Jaeger et al. “Optimization and applications of echo state networks with leaky-integrator neurons”. In: *Neural Networks* 20.3 (2007), pp. 335–352.
- [35] G. Tanaka et al. “Recent advances in physical reservoir computing: A review”. In: *Neural Networks* 115 (2019), pp. 100–123.
- [36] Y. Kawai, J. Park, and M. Asada. “A small-world topology enhances the echo state property and signal propagation in reservoir computing”. In: *Neural Networks* 112 (2019), pp. 15–23.
- [37] W. Maass, T. Natschläger, and H. Markram. “Real-time computing without stable states: A new framework for neural computation based on perturbations”. In: *Neural Computation* 14.11 (2002), pp. 2531–2560.
- [38] M. Dale et al. “Reservoir computing quality: connectivity and topology”. In: *Natural Computing* 20 (2021), pp. 205–216.
- [39] Y. Bouhadjar et al. “Sequence Learning, Prediction, and Replay in Networks of Spiking Neurons”. In: *PLoS Computational Biology* 18.6 (June 2022). Ed. by S. Kiebel, e1010233. ISSN: 1553-7358. DOI: 10.1371/journal.pcbi.1010233. (Visited on 07/25/2022).
- [40] J. J. Bolhuis and M. Gahr. “Neural mechanisms of birdsong memory”. In: *Nature Reviews Neuroscience* 7.5 (May 2006), 347–357. ISSN: 1471-0048. DOI: 10.1038/nrn1904. URL: <http://dx.doi.org/10.1038/nrn1904>.
- [41] R. H. Hahnloser and A. Kotowicz. “Auditory representations and memory in birdsong learning”. In: *Current Opinion in Neurobiology* 20.3 (June 2010), 332–339. ISSN: 0959-4388. DOI: 10.1016/j.conb.2010.02.011. URL: <http://dx.doi.org/10.1016/j.conb.2010.02.011>.
- [42] M. S. Fee, A. A. Kozhevnikov, and R. H. Hahnloser. “Neural mechanisms of vocal sequence generation in the songbird”. In: *Annals of the New York Academy of Sciences* 1016.1 (2004), pp. 153–170.
- [43] G. F. Lynch et al. “Rhythmic continuous-time coding in the songbird analog of vocal motor cortex”. In: *Neuron* 90.4 (2016), pp. 877–892.
- [44] M. Konishi. “The role of auditory feedback in the control of vocalization in the white-crowned sparrow 1”. In: *Zeitschrift für Tierpsychologie* 22.7 (1965), pp. 770–783.
- [45] S. M. Gobes and J. J. Bolhuis. “Birdsong Memory: A Neural Dissociation between Song Recognition and Production”. In: *Current Biology* 17.9 (May 2007), 789–793. ISSN: 0960-9822. DOI: 10.1016/j.cub.2007.03.059. URL: <http://dx.doi.org/10.1016/j.cub.2007.03.059>.
- [46] J. J. Bolhuis and S. Moorman. “Birdsong memory and the brain: In search of the template”. In: *Neuroscience & Biobehavioral Reviews* 50 (Mar. 2015), 41–55. ISSN: 0149-7634. DOI: 10.1016/j.neubiorev.2014.11.019. URL: <http://dx.doi.org/10.1016/j.neubiorev.2014.11.019>.
- [47] M. H. Kao, A. J. Doupe, and M. S. Brainard. “Contributions of an avian basal ganglia–forebrain circuit to real-time modulation of song”. In: *Nature* 433.7026 (2005), pp. 638–643.
- [48] D. Aronov, A. S. Andalman, and M. S. Fee. “A specialized forebrain circuit for vocal babbling in the juvenile songbird”. In: *Science* 320.5876 (2008), pp. 630–634.
- [49] M. Fee and J. Goldberg. “A hypothesis for basal ganglia-dependent reinforcement learning in the songbird”. In: *Neuroscience* 198 (Dec. 2011), 152–170. ISSN: 0306-4522. DOI: 10.1016/j.neuroscience.2011.09.069. URL: <http://dx.doi.org/10.1016/j.neuroscience.2011.09.069>.
- [50] V. Gadagkar et al. “Dopamine neurons encode performance error in singing birds”. In: *Science* 354.6317 (2016), pp. 1278–1282.
- [51] M. Wehr and A. M. Zador. “Balanced inhibition underlies tuning and sharpens spike timing in auditory cortex”. In: *Nature* 426.6965 (2003), pp. 442–446.
- [52] L. Gabernet et al. “Somatosensory integration controlled by dynamic thalamocortical feed-forward inhibition”. In: *Neuron* 48.2 (2005), pp. 315–327.
- [53] M. N. Shadlen and W. T. Newsome. “Noise, neural codes and cortical organization”. In: *Current Opinion in Neurobiology* 4.4 (1994), pp. 569–579.
- [54] C. Van Vreeswijk and H. Sompolinsky. “Chaos in neuronal networks with balanced excitatory and inhibitory activity”. In: *Science* 274.5293 (1996), pp. 1724–1726.
- [55] Y. Shu, A. Hasenstaub, and D. A. McCormick. “Turning on and off recurrent balanced cortical activity”. In: *Nature* 423.6937 (2003), pp. 288–293.
- [56] B. Haider et al. “Neocortical network activity in vivo is generated through a dynamic balance of excitation and inhibition”. In: *Journal of Neuroscience* 26.17 (2006), pp. 4535–4545.
- [57] M. Abeles. *Local Cortical Circuits: An Electrophysiological study*. Springer, Berlin, 1982.
- [58] M. Abeles. *Corticonics: Neural Circuits of the Cerebral Cortex*. Cambridge University Press, 1991.
- [59] E. Bienenstock. “A model of neocortex”. In: *Network: Computation in Neural Systems* 6.2 (1995), pp. 179–224.
- [60] M. Diesmann, M.-O. Gewaltig, and A. Aertsen. “Stable propagation of synchronous spiking in cortical neural networks”. In: *Nature* 402.6761 (1999), pp. 529–533.

- [61] J. Kremkow, A. Aertsen, and A. Kumar. “Gating of signal propagation in spiking neural networks by balanced and correlated excitation and inhibition”. In: *Journal of Neuroscience* 30.47 (2010), pp. 15760–15768.
- [62] M. A. Petrovici et al. “Characterization and compensation of network-level anomalies in mixed-signal neuro-morphic modeling platforms”. In: *PloS One* 9.10 (2014), e108590.

Acknowledgment

We thank all members of the NeuroTMA and the CompNeuro labs for many insightful discussions. Additionally, we are grateful to Richard Hahnloser and his lab for valuable feedback on learning in songbirds. We gratefully acknowledge funding from the European Union for the Human Brain Project under the grant agreement 945539, the Manfred Stärk Foundation and the Swiss National Science Foundation (SNSF) for the “Prospective coding with pyramidal neurons”-grant (310030L.156863) and the Sinergia Grant “Neural Processing of Distinct Prediction Errors: Theory, Mechanisms & Interventions” (CRSII5.180316). Our work has greatly benefitted from access to the Fenix Infrastructure resources, which are partially funded from the European Union’s Horizon 2020 research and innovation programme through the ICEI project under the grant agreement No. 800858.

Author contributions

KV, MAP and WS designed the model. KV wrote the initial code for the software simulation which was extended and adapted by LK. The experiments were jointly designed by LK, KV, BvH, FB, WS and MAP and conducted by LK and KV. All authors contributed to the writing of the manuscript.

Code availability

Code for the simulations is available at https://github.com/unibe-cns/temporal_sequence_learning.

Competing Interests statement

The authors declare no competing interests.

Supplementary Information

Pattern replay after disruptions

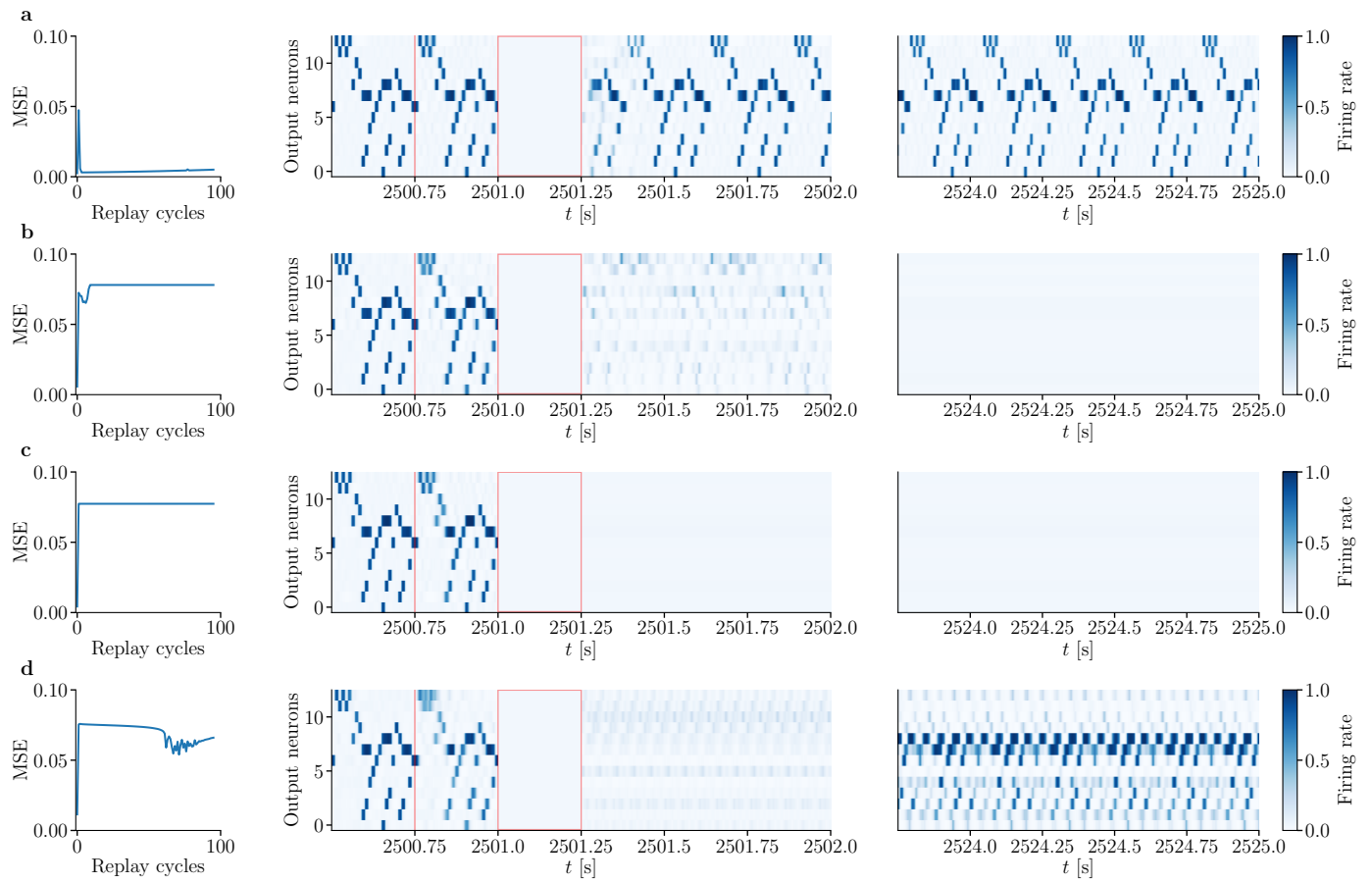


Figure 7: Selected runs with disrupted replay of Fig. 5. Left column: MSE error during replay. Middle: Activity in output population at the beginning of the replay phase (red line marks the end of nudging). Right: Activity during the last replay cycles.

Simulation parameters

Table 1: Parameters for simulations.

	Fig. 2	Fig. 3 (c) ⁽¹⁾	Fig. 5 + Fig. 7	Fig. 4 (a+b)	Fig. 4 (c+d)
dt [ms]	10^{-1}	10^{-1}	10^{-1}	10^{-1}	10^{-1}
Training cycles	10^4	10^4	10^4	10^4	up to 3×10^4
Replay cycles	100	10	100	100	100
Validation interval	20	20	20	20	20
Output neurons	13	13	13	13	13
Latent neurons	[30, 50, 100]	50	50	50	50
p	0.2	0.2	0.2	0.1 – 0.5	0.2
p_0	0.04	0.04	0.04	0.04	0.04
q	0.15	0.15	0.15	0.05 – 0.25	0.15
Dendritic sparsity	all-to-all	all-to-all	all-to-all	all-to-all	0.3 – 0.8
C_m^{den}	1	1	1	1	1
C_m^{som}	1	1	1	1	1
E_l	-70	-70	-70	-70	-70
E_{exc}	0	0	0	0	0
E_{inh}	-75	-75	-75	-75	-75
g_l [ms^{-1}]	0.1	0.1	0.1	0.1	0.1
g_{den} [ms^{-1}]	2.0	2.0	2.0	2.0	2.0
$g_{\text{exc},0}$ [ms^{-1}]	0.3	0.3	0.3	0.3	0.3
$g_{\text{inh},0}$ [ms^{-1}]	6.0	6.0	6.0	6.0	6.0
$a^{(2)}$	0.3	0.3	0.3	0.3	0.3
$b^{(2)}$	-58	-58	-58	-58	-58
d^{den} [ms]	$\mathcal{U}[5, 15]$	$\mathcal{U}[5, 15]$	$\mathcal{U}[5, 15]$	$\mathcal{U}[5, 15]$	$\mathcal{U}[5, 15]$
$d_{\text{exc}}^{\text{som}}$ [ms]	$\mathcal{U}[5, 15]$	$\mathcal{U}[5, 15]$	$\mathcal{U}[5, 15]$	$\mathcal{U}[5, 15]$	$\mathcal{U}[5, 15]$
δ [ms]	25	25	25	25	25
Init $\mathbf{W}_{\text{out},\text{out}}$ [ms^{-1}]	$\mathcal{N}(0, 0.5)$	$\mathcal{N}(0, 0.5)$	$\mathcal{N}(0, 0.5)$	$\mathcal{N}(0, 0.5)$	$\mathcal{N}(0, 0.5)$
Init $\mathbf{W}_{\text{out},\text{lat}}$ [ms^{-1}]	$\mathcal{N}(0, 0.5)$	$\mathcal{N}(0, 0.5)$	$\mathcal{N}(0, 0.5)$	$\mathcal{N}(0, 0.5)$	$\mathcal{N}(0, 0.5)$
Init $\mathbf{W}_{\text{lat},\text{out}}$ [ms^{-1}]	$\mathcal{N}(0, 0.5)$	$\mathcal{N}(0.19, 5.7)$	$\mathcal{N}(0, 0.5)$	$\mathcal{N}(0, 0.5)$	$\mathcal{N}(0, 0.5)$
Init $\mathbf{W}_{\text{lat},\text{lat}}$ [ms^{-1}]	$\mathcal{N}(0, 0.5)$	$\mathcal{N}(0.08, 6.1)$	$\mathcal{N}(0, 0.5)$	$\mathcal{N}(0, 0.5)$	$\mathcal{N}(0, 0.5)$
η_o [ms^{-2}]	10^{-4}	4×10^{-3}	10^{-4}	10^{-4}	10^{-4}
η_l [ms^{-2}]	10^{-3}	$4 \times 10^{-2(3)}$	10^{-3}	10^{-3}	10^{-3}

¹ Parameters for Fig. 3 (b) are the same as for Fig. 2.

² $r = \varphi(u) = \frac{1}{1 + \exp a(b-u)}$

³ In the reservoir-like network only the connections within the output population and the ones from the latent to the output population learn.